PHYSICAL REVIEW E **67**, 031606 (2003)

Dissipating step bunches during crystallization under transport control

Hong Lin,[2] S.-T. Yau,[3] and Peter G. Vekilov[1,*]
[1]*Department of Chemical Engineering, University of Houston, Houston, Texas 77204*
[2]*Center for Microgravity and Materials Research, University of Alabama in Huntsville, Huntsville, Alabama 35899*
[3]*Department of Physics, Hunter College, CUNY, New York 10021*

(Received 15 August 2002; published 25 March 2003)

In studies of crystal formation by the generation and spreading of layers, equidistant step trains are considered unstable—bunches and other spatiotemporal patterns of the growth steps are viewed as ubiquitous. We provide an example to the opposite. We monitor the spatiotemporal dynamics of steps and the resulting step patterns during crystallization of the proteins ferritin and apoferritin using the atomic force microscope. The variations in step velocity and density are not correlated, indicating the lack of a long-range attraction between the steps. We show that (i) because of its coupling to bulk transport, nucleation of new layers is chaotic and occurs at the facet edges, where the interfacial supersaturation is higher; (ii) step bunches self-organize via the competition for supply from the solution; and, (iii) bunches of weakly interacting steps decay as they move along the face. Tests by numerical modeling support the conclusions about the mechanisms underlying our observations. The results from these systems suggest that during crystallization controlled by transport, with weakly or noninteracting growth steps, the stable kinetic state of the surface is an equidistant step train, and step bunches only arise during nucleation of new layers. Since nucleation only occurs at a few sites on the surface, the surface morphology may be controllably patterned or smoothened by locally controlling nucleation.

DOI: 10.1103/PhysRevE.67.031606 PACS number(s): 81.10.Aj

I. INTRODUCTION

During crystallization by spreading of layers, the dominant mode of growth from a broad range of media—high and low temperature solutions, vapors, etc.—the growth steps have been found to break from an equidistant arrangement, leading to bunches and higher-order patterns [1–5]. Historically, interest in step-bunch formation has been spurred by their link to striations, nonuniform defect incorporation, and other inhomogeneities that ruin the quality and utility of the crystals [4,6]. On the other hand, it has recently been suggested that step bunches could be utilized as suitable sites for the nucleation of nanometer-size islands on the surface of foreign substrates; a self-organizing step-bunch pattern would serve as a template for an ordered array of such islands [7,8]. These two features underscore the pursuit of insight into the mechanisms of formation and evolution of step bunches. Such insight would serve as the basis of control pathways that allow in some cases to either completely avoid step bunching, to constrain bunching to an unavoidable minimum, or, for certain systems, to induce preselected step patterns.

The theoretical treatments of the bunching of steps start from the loss of stability of an equidistant step train [9–15]. These works consider steps on the surfaces of crystals growing or dissolving in solution, melt, vapor, or high-vacuum environments. Steps are assumed to interact through competition for supply via the adsorbed surface layer [11], or via the bulk of the source phase [9,10,14]. Other sources of step interaction include steps' elastic fields [12], and entropy associated with the finite width that a meandering step occupies [3]. Steady and time-dependent impurity effects [13,14,16] and various types of asymmetry of incorporation of the building blocks into the steps have been included in the models [8,11,12,15,17]. The general conclusion of these works is that the equidistant step trains are unstable, and step bunching is ubiquitous. A corollary of most of these mechanisms is that as steps propagate away from their source towards the edge of the crystal, bunching is expected to escalate.

Here, we provide an example to the opposite. We show that during crystallization of the proteins ferritin and apoferritin, chaotic generation of layers by a highly nonlinear surface nucleation is followed by self-organization of these layers into regular step-bunch patterns. As they propagate along the surface, the step bunches decay, i.e., the stable state of the vicinal slope is that of an equidistant step train. We assign the stability of the equidistant step train to two factors: the lack of a long-range attraction between the steps, and the dominant role of transport through the solution in the overall control of the crystallization kinetics.

We found no differences in the kinetic dependences recorded with ferritin and apoferritin. Moreover, a parallel study revealed that the two proteins not only have identical growth mechanisms [18], but also their solubilities and kinetic coefficients for incorporation into the steps rescaled in terms of molecular densities and sizes are identical [19]. Because of this identity, in the following discussion results for the two proteins will be used interchangeably.

II. EXPERIMENTAL SECTION

A. Solution preparation

Ferritin and apoferritin stock solutions were separated into monomer, dimer, and "trimer" fractions as described in

---

[*] Corresponding author. FAX: 713 743-4323. Email address: vekilov@uh.edu

detail in Ref. [20]. All experiments discussed here were carried out using the monomer fraction dissolved in 0.2 M sodium acetate buffer at pH 5.0. The sum residual amount of dimer and trimers in this fraction after purification was ~5% (w/w). To induce crystallization, $CdSO_4$ was added to concentration in the crystallizing solution of 2.5% (w/v). The supersaturation of the solution was calculated as $\sigma = \Delta\mu/k_B T = \ln(\gamma C/\gamma_e C_e) \approx \ln(C/C_e)$. Here C is the solution concentration, the concentration at equilibrium $C_e = 25\ \mu\mathrm{g\,mL}^{-1}$ for apoferritin, and $35\ \mu\mathrm{g\,mL}^{-1}$ for ferritin. This C_e was determined from atomic force microscopy monitoring of step motion as the value at which the propagation of the steps stops, before reversing direction at lower concentrations [18,21,22]. The last approximate equality above uses that the activity coefficients $\gamma \approx \gamma_e \approx 1$, demonstrated in Ref. [23].

B. Crystallization and atomic force microscopy imaging

Droplets of crystallizing solution of ~50 μL of either protein were placed on 12-mm glass coverslips mounted on iron disks. To avoid evaporation the droplets were covered with glass covers, hermetically sealed and left overnight in a controlled room temperature at ~22 °C. Typically, this lead to the formation of 3–20 crystals of sizes ranging from 20 to 200 μm, firmly attached to the glass bottom. Disks with droplets containing 3–5 crystals were selected and magnetically mounted on the AFM scanner. The fluid AFM cell was filled with crystallizing solution before imaging commenced.

All images were collected *in situ* during growth of the crystals using the less intrusive tapping mode of imaging [24]. This allows visualization of adsorbed protein and impurity species (tip impact in contact imaging mode often prevents such imaging). We also employed scans with disabled y axis, similar to previous STM work on metals and semiconductors in ultrahigh vacuum [25]. The technique allows continuous monitoring of processes with characteristic times of the order of 0.1–1 sec.

We used standard SiN tips. The tapping drive frequency was adjusted in the range 25–31 kHz to the resonance value for specific tip used. Other scanning parameters were adjusted such that continuous imaging affected neither the surface structure, nor the process dynamics. For verification, we varied the scan sizes and the time elapsed between image collections, and saw that neither the spatial nor the temporal characteristics of the processes changed. For further details of the AFM imaging, see Refs. [21, 26, 27].

III. RESULTS AND DISCUSSION

A. Phenomenology of the step patterns

Figure 1 illustrates the typical surface morphology of a large, ~450 μm apoferritin crystal growing from a supersaturated solution of this protein. We see two locations of the same train of steps: near the facet edge in Fig. 1(a) where new layers are generated by surface nucleation of islands, and, in Fig. 1(b), near the center of the facet, ~250 μm downstream. At both locations, layer thickness equals the lattice parameter in the ⟨111⟩ direction, 10.5 nm [21]. While the step generation near the edge appears chaotic, with single steps intermingled with stacks of layers of various height, down the steps' pathway, a regular step arrangement evolves, consisting of near-perfect step-density waves, Fig. 1(d).

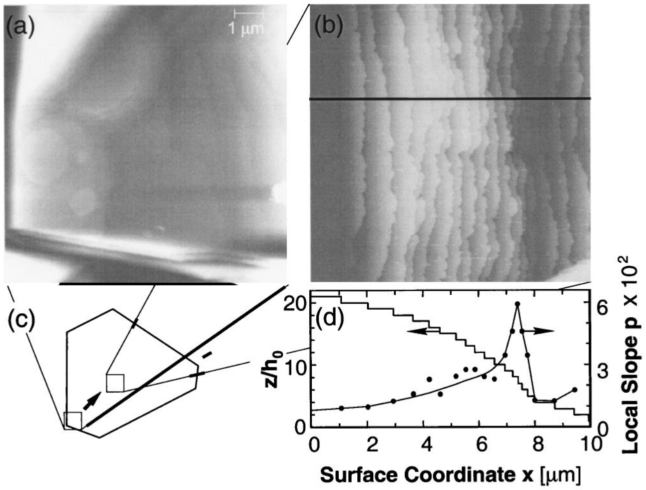

FIG. 1. Step patterns on the surface of a ferritin crystal. (a) and (b) atomic force microscopy images of areas located near the facet edge in (a) and close to the facet center (b). The areas of (a) and (b) were chosen so that the steps seen in (b) are generated at the location imaged in (a). (c) Schematic of crystal face and locations of imaging in (a) and (b); arrow indicates direction of step motion in monitored step train. (d) Height profile and local slope distribution along the line shown in (b); $h_0 = 10.6$ nm is the height of a monomolecular step on the [111] surface of the ferritin crystals.

The reasons for the selection of the edges as a preferred surface nucleation site are revealed by the numerical modeling of the convective-diffusive transport in a supersaturated solution of the proteins ferritin and apoferritin towards a growing crystal of the respective protein in Ref. [28]. The results showed a significant nonuniformity of the supersaturation at the crystals' surface [28]. In agreement with theory and previous observations [29,30], these simulations predict a higher supersaturation σ at the crystal edges than at the centers of the facets. The ratios of the σ values at the two locations depend on the transport regime (convective diffusive or purely diffusive), crystal's size, and supersaturation, but were always between ~1.5 and ~3 [28]. The changes in morphology induced by higher supersaturations and larger crystal sizes, illustrated in Fig. 2, are in agreement with the simulations' results—on crystals smaller than ~100 μm and at low supersaturations, step generation is uniformly distributed over the whole crystal facet, indicating supersaturation uniformity. As the crystals grow and the facet width exceeds 100 μm, step generation gradually concentrates along the crystal edges Fig. 2(b). For crystals larger than ~150–160 μm in Fig. 2(c), layer generation occurs exclusively along the edges.

B. Spatiotemporal evolution of step patterns

For insight into the step pattern dynamics, we monitored the spatiotemporal evolution of sections of the step train. For this, we chose a fast scanning direction perpendicular to the

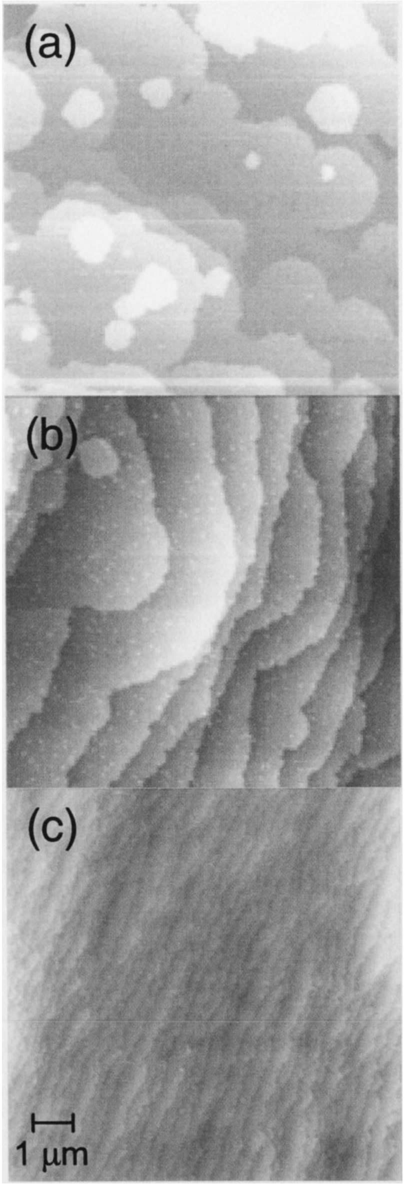

FIG. 2. Atomic force microscopy images of the surface of growing apoferritin crystals taken near the center of the respective facet. Facet size is ~90 μm in (a), ~150 μm in (b) and ~220 μm in (c).

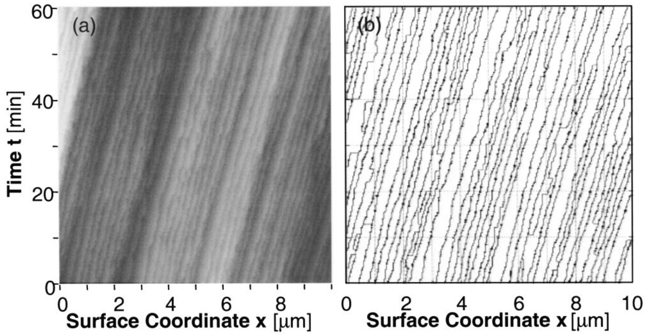

FIG. 3. Quantification of the step train dynamics. (a) A pseudoimage of a 10 μm section of a step train similar to the one in Fig. 2(c) recorded by orienting the fast scanning axis perpendicular to the dominant step direction, see, e.g., Fig. 2(c), and disabling the slow scanning axis of the atomic force microscope. In this imaging mode, the vertical axis represents the elapsed time. (b) Digital version of the image in (a) in which each point represents the position of a step along the surface coordinate x at time t.

steps and disabled the slow scanning axis of the AFM. In the collected pseudoimages, the vertical axis represents time. The duration of such data collections were often as long as 90–100 min; after the end of such runs, area scans that include the line of scanning in the x-t mode were collected. Some (<20%) of these images, especially those collected in earlier experiments, revealed artifacts due to tip impact along the single scanning line; only x-t data sets without such artifacts were considered. An example of such data is shown in Fig. 3(a). The digitized pseudoimage in Fig. 3(b) consists of lines that trace the location x of each step in Fig. 3(a) at time t. These lines fully characterize the dynamics of the monitored step train segment. Thus, the slope of a line tracing a step is reciprocal to the step velocity v, the local step density l^{-1}, and vicinal slope $p = h_0 l^{-1}$ [$h_0 = 10.5$ nm is the thickness of a (111) layer in ferritin or apoferritin] can be determined from the distances between the lines l at a chosen time t. The time intervals between subsequent steps Δt at a chosen location x determine the normal growth rate $R = h_0/\Delta t$ at this location.

Figure 3(b), similar plots in Fig. 4, and all other similar data sets show that the step density varies within a broad range. Steps in packets of high step density do not have lower or higher step velocities than those in packets of lower density, i.e., the step bunches move with a velocity similar to that of the elementary steps. Accordingly, plots of the local step velocities as a function of the step density surrounding these steps (graphs not shown) for all x-t data sets reveal no correlation between the two variables. We conclude that

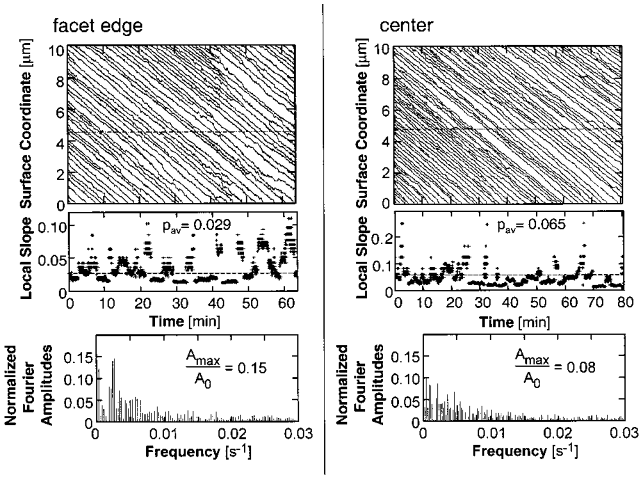

FIG. 4. Spatiotemporal characteristics of the step trains at supersaturation $\sigma = 2.3$ near the facet edge and center, as indicated on the top of each column. Top pannels, x-t diagrams of the step train sections. Middle, time traces of the local vicinal slope at the middle of each segment; the time-averaged slope is printed in the plots. These traces correspond to cross sections of the x-t diagrams marked with dashed lines. Bottom, Fourier transforms of the slope traces; the value of the maximum normalized amplitude is printed.

there exists no long-range step-step attraction or repulsion in the ferritin or apoferritin system.

Careful observation of the step traces in Fig. 3(b) reveals numerous twinning (two step joining into a single one) and detwining events. Only steps separated prior to twinning by distances of <100 nm≈ 7 lattice parameters twin, indicating the presence of a short-range step-step attraction. In Ref. [18], it was shown that this attraction is likely due to the overlapping of the fields of surface diffusion of adjacent steps; the characteristic surface diffusion length, determined from these results, was a few lattice parameters. This short length determines the range of the attraction. The numerous twinning events suggest that the repulsion between steps that may be associated with entropic or elastic interactions, often present in semiconductor systems [3,12], is weaker than the attraction.

Detwinning, or splitting of double-height steps into two elementary steps will be addressed further below.

C. Mechanisms of step pattern formation and evolution

Figure 4 compares the spatiotemporal characteristics of step patterns at the crystal periphery, and at the facet center. The studied crystal, similar to the one depicted in Fig. 1 above, was about 400 μm in size, with steps generated at the edges of the facet and moving inwards. The two top panels are the respective *x-t* diagrams. The corresponding time evolutions of the vicinal slope at the middle of the monitored step train segments are shown in the middle panels. Comparisons between these traces, and between their respective Fourier transforms in the bottom panels of Fig. 4 show that as the steps move, the variations in local slope decrease. This decrease occurs despite the increase in the average value of the vicinal slope—higher slope is considered a destabilizing factors that favors the formation of step bunches [31,32], and it contrasts the behavior of the step patterns in another well-investigated protein system, lysozyme [33,34].

We attribute the higher vicinal slope at the facet center to the lower supersaturation at this location, according to the mechanism put forth in Ref. [35]; for experimental evidence in favor of this mechanism, including for other protein systems, see Refs. [30, 36]. Note that the slope increases from facet edge to center by a factor of ~2, roughly equal to the corresponding decrease in interfacial supersaturation. This latter observation is consistent with the above conclusion about the lack of long-range step-step attraction—such attraction leads to vicinal slope increase severalfold stronger than the supersaturation decrease causing it [36].

The Fourier spectra in the bottom panels of Fig. 4 show a sharp peak in the data collected near the edge. These peaks indicate that soon after the chaotic layer generation seen in Fig. 1, the steps self-organize into rather regular patterns. There are no definite peaks in the Fourier spectra of the data for the facet center, indicating partial suppression of instabilities. The step-bunch decay, reflected by the data in Fig. 4, reveals a tendency towards equidistant steps, i.e., the equidistant step train is the stable state of the step train in the conditions of growth in Fig. 4.

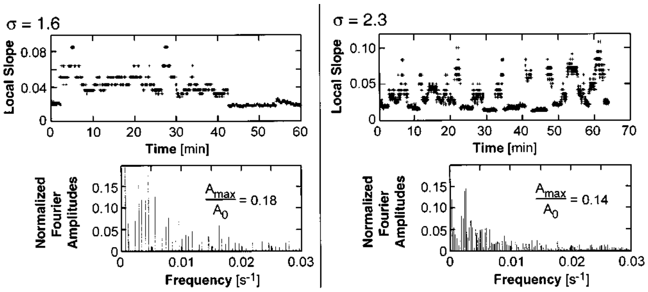

FIG. 5. Spatiotemporal characteristics of the step trains near the facet periphery at the supersaturations indicated on the top of each column. Top, time traces of the local vicinal slope extracted from the respective *x-t* diagrams (not shown). Bottom, Fourier transforms of the slope traces; the value of the maximum normalized amplitude is printed.

Figures 5 and 6 reveal that the fluctuations in the vicinal slope decrease with increasing supersaturations, and with larger crystal sizes. The right-hand side panels in Fig. 6, reflecting data collected at the facet center of a crystal ~400 μm wide show significantly reduced slope fluctuations and step bunching. The size of the crystal, the supersaturation, and the location of sampling on the facet are the parameters, which determine the rate of transport of solute to the studied step segment at the interface [33,37]. Furthermore, higher supersaturations, larger sizes, and central locations are conducive to stronger transport control of the overall process rate. In this context, the observations in Figs. 4, 5, and 6 suggest that the coupling of bulk solution transport to interfacial kinetics causes step bunching in the ferritin or apoferritin system.

To determine which of the two coupled processes has a higher weight in the overall kinetics control for the case of ferritin or apoferritin, we calculate the kinetic Peclet number, Pe_k for the ferritin or apoferritin system,

$$\mathrm{Pe}_k = \beta_{st} p\, \delta / D, \tag{1}$$

where β_{st} is the step kinetic coefficient, δ is a characteristic length of the bulk diffusion, typically a few hundred micrometers, and D is the diffusivity of ferritin,

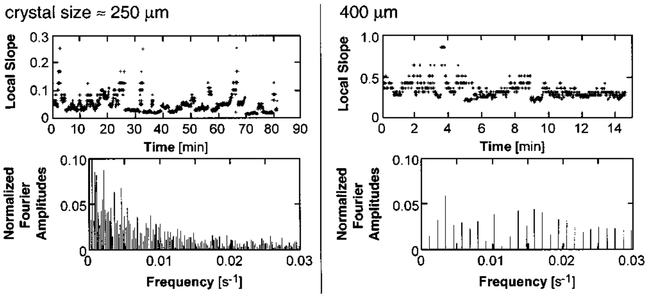

FIG. 6. Spatiotemporal characteristics of the step trains at supersaturation $\sigma = 2.3$ recorded at the facet center with crystals whose sizes are indicated on the top of each column. Top, time traces of the local vicinal slope extracted from the respective *x-t* diagrams (not shown). Bottom, Fourier transforms of the slope traces.

equal to that of apoferritin, $D=3.2\times10^{-7}$ cm^2 s^{-1}. [19] With $\beta_{st}=6\times10^{-4}$ cm s^{-1} for both proteins [18,20] and taking, as in Refs. [5, 33], $\delta=300$ μm, Pe$_k\cong1.1$. Values of Pe$_k\geqslant1$ indicate higher weight of the transport through the solution bulk in the overall control of the kinetics. This conclusion agrees with the heavy solution depletion at the crystal-solution interface that brings the interfacial concentration of the protein down to only $\sim$30% of its value far from the crystal [28].

Thus, the tendencies illustrated by Figs. 5 and 6 agree with a rationale put forth earlier [5,33], which predicts that in transport-controlled systems, higher weight of transport leads to lower kinetic instabilities.

The scenario of the formation and evolution, emerging from the above observations and considerations, is as follows: The coupling of the surface nucleation process, with its exponential dependence on supersaturation, to the slow supply of solute to the nucleation sites leads to a kinetic instability with quasiperiodically changing rates [38]. The actual near-chaotic picture, seen in Fig. 1(a), will be discussed below. Since step velocity only has a weak linear dependence on supersaturation, it is less sensitive to these perturbations, and as the steps move inwards, step patterns can become more regular. Since steps separated from their neighbors are in better supply conditions [37], they move faster until the well-organized step-density wave, illustrated in Figs. 1(b) and 1(c) sets in.

D. Decay of the step bunches in a transport-controlled regime

To understand the decay of step bunches in the transport-controlled regime, we invoke a scenario similar to the one put forth in Refs. [2,10,32]. Areas of high density of noninteracting steps are also areas of local growth rate maxima and, in a transport-controlled regime, supersaturation minima. Again, in a transport-controlled regime, the solute diffusion field near the interface lags behind the step pattern that generates it. As a consequence, step train segments of high step density move into areas of higher supersaturation, while the trailing segments of lower step density finds themselves in areas of lower supersaturation. The steps trailing behind the step bunch are prevented from catching up with the bunch and increasing its height. A self-consistent analytical solution has shown that this results in dissipating step bunches and stabilization of the equidistant step trains [32].

A crucial detail in the above mechanism is the lack of long-range step-step attraction, discussed in a preceding subsection—such attraction would impede step train segments of high step density stronger than the acceleration due to growth under dominant transport control. Thus, the ultimate cause for the stability of equidistant step trains in ferritin or apoferritin growth is the short characteristic length of surface diffusion. Further insight into the reasons underlying the selection of such short characteristic length is inhibited by our poor understanding of the adsorption and desorption processes and the nature of the adsorbed layer; for additional data on surface diffusion on ferritin crystal faces incompatible with the classical models, see Ref. [18].

E. Numerical modeling

To test the feasibility that the mechanism described above could underlie the observed unsteady behavior in the ferritin or apoferritin system, we carried out numerical simulations. We used the finite-volume numerical model of the bulk transport in solution coupled to the crystal growth kinetics at the interface discussed in detail in Refs. [37,39]. For simplicity, only purely diffusive transport was considered, for justification and the limits of the relevance of this assumption, see Ref. [39]. The model is two dimensional, with a crystal of $2a$ long and a high (a was set between 100 and 400 μm) resting at the bottom center of a rectangular cell 1 mm high and 6 mm wide. To maximize the spatial resolution in the calculation of the solute flux towards individual steps, we used a mesoscale grid at the solution-crystal interface. This grid contains 10 vertical mesh lines per terrace that moves with the step positions and adjust to the changing terrace widths during the simulation, keeping high line density near the steps and lower density in the middle of the terrace. The mesoscale grid contains 11 horizontal lines, which start at a distance of 0.22 μm from the interface and have spacings increasing by a power law to 25 μm. The protein concentrations and fluxes towards the solution crystal interface, calculated within the mesoscale grid, are continuously coupled to those in the macroscale grid as discussed in Ref. [37].

This model was evaluated with transport and kinetics parameters characteristic for the growth of ferritin and apoferritin crystals from aqueous solutions. The velocity of each step ν was assumed to be proportional to the local, time-dependent protein concentration at the interface $C(x,t)$:

$$\nu(x,t)=\beta_{\text{step}}\Omega C_e[C(x,t)-C_e]. \tag{2}$$

This assumption implies that the parameter of interstep interaction $k=0$ (for the link between k and the parameters of the surface diffusion and the direct incorporation mechanisms, see Refs. [39,40]), based on the evidence discussed in relation to Fig. 3. In Eq. (2.) $\Omega=\frac{1}{4}b^3=1.56\times10^{-18}$ cm^3 is the volume occupied by one molecule in the crystal; $b=18.4$ nm [41] is the lattice parameter of the f.c.c. lattice of ferritin or apoferritin crystals, $C_e=3\times10^{13}$ cm^{-3} is the solubility in units of molecules per unit volume, so that $\Omega C_e=5\times10^{-5}$. The kinetic coefficient β_{step} was taken to be 6×10^{-4} cm s^{-1}, Refs. [21, 22].

Since we are interested in modeling step generation and propagation on larger crystals, following Figs. 1 and 2, we assume that nucleation of new layers only occurs at the edges of the facets. As in Refs. [37,39], we assume that the rate of surface nucleation $J_{2\text{D}}$ depends on the time-dependent protein concentration $C_{\text{corner}}(t)$ and the solution supersaturation $\sigma_{\text{corner}}(t)=\ln[C_{\text{corner}}(t)/C_e]$ as

$$J_{2\text{D}}(t)=AC_{\text{corner}}(t)\exp\left(-\frac{B}{\sigma_{\text{corner}}(t)}\right). \tag{3}$$

The value of the phenomenological parameter A (for its link to the actual nucleation parameters, see Refs. [37,39]), was varied to ensure continuity or to vary the discontinuity between the initial surface condition and the newly emerging

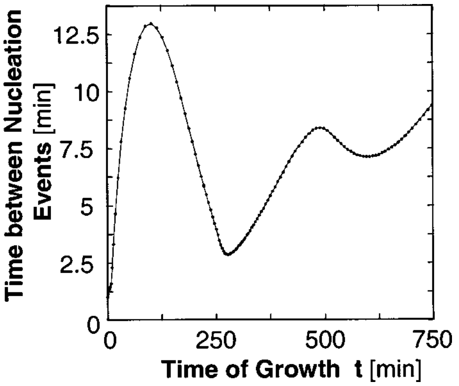

FIG. 7. Numerical modeling results for a crystal with upper facet size $2a=250\ \mu$m. The time between individual events of nucleation of new layers at the edge of the top facet are plotted as a function of the growth time.

steps. The constant B contains the energy barrier for nucleation, and its value was set at 60 [27,39].

The probability P for the generation of a new step within a time t_{nucl} after the preceding nucleation event was calculated as [42]

$$P[t_{\mathrm{nucl}},C_{\mathrm{corner}}(t)]=1-\exp\{-J_{2\mathrm{D}}[C_{\mathrm{corner}}(t)]t_{\mathrm{nucl}}\}, \quad (4)$$

and a nucleation event occurred only after P exceeded a predetermined value, selected as in Ref. [39]. Since C_{corner} drops immediate after the generation of a step and is slowly replenished from the solution bulk, Eq. (4) provides for a self-coordinated step pattern generation.

The initial state of the crystal surface is an equidistant step train with slope $p=0.02$ and the highest point at the two edges of the two-dimensional crystal. At the beginning of a simulation, the crystal is exposed to solution with concentration 0.25 mg mL$^{-1}=10C_e$, so that $\sigma=2.3$. As the steps begin to move according to Eq. (2), the solution is depleted and the interfacial concentration drops. This leads to lower nucleation rate, according to Eq. (3), and to longer times between individual nucleation events. This behavior is illustrated by the first 120 min in Fig. 7. The slower growth at time of growth ~120 min allows replenishment of protein concentration in the interfacial layer, and nucleation gradually accelerates, until the oscillation is repeated with a lower amplitude. No steady state is reached for simulation times longer than 2000 min of growth.

Note the emergence of two characteristic nucleation times linked to the slow supply of solute from the solution. The shorter one separates the individual nucleation events according to Eq. (4), while the longer one describes the long-term variation of the nucleation rate in Fig. 7. In simulations of kinetics-controlled systems, only the first time is present and the nucleation reaches a quasisteady state [37,43].

If the top face half size a is greater than 150 μm, solution depletion and growth deceleration is faster. Solution depletion reaches lower levels, causing the nucleation of new layers and growth to stop. With 150 $\mu\mathrm{m}<a<200\ \mu$m, nucleation resumes after 150–200 min; with $a>200\ \mu$m, growth did not resume for up to 1000 min. With $a<100\ \mu$m, the minimum of the time between nucleation events, which in Fig. 7 occurs at ~120 min, is not reached for 1000 min of simulations.

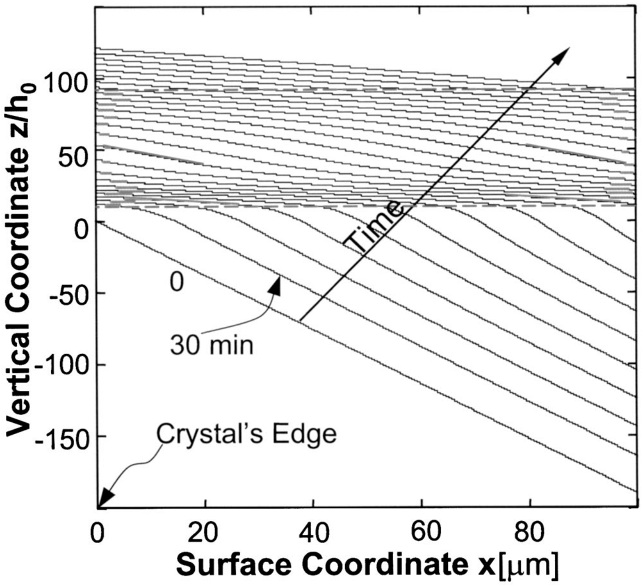

FIG. 8. Numerical modeling results for a crystal with upper facet size $2a=250\ \mu$m. Evolution of the left section of the crystal surface profile as a result of the spreading of the layers whose generation is reflected in Fig. 7; the time interval between subsequent profiles is 30 min. $h_0=10.6$ nm is the height of a monomolecular step on the [111] surface of the ferritin and apoferritin crystals. $z/h_0=0$ corresponds to the facet edge at $t=0$. Horizontal dashed lines bracket steps used for comparisons. Inclined lines mark pairs of parallel lines of equal length. Deviation of the step profile from the right inclined lines illustrates the slight steepening of the step train. Short horizontal lines mark the rightmost and leftmost visible terrace widths; their spread is between 1.5 and 5.3 μm at the facet edge and 1.4 and 4.9 μm at $x\sim 90\ \mu$m, indicating a tendency towards dissipation of the step bunch and equalization of interstep distances.

The oscillatory nucleation rate in Fig. 7 qualitatively explains some of the features of the unsteady nucleation, observed in Figs. 1 and 2. Thus, high nucleation rate and short times between nucleation events would correspond to the nucleation of stacks of new layers, while the long times between nucleation events results in the regions of low step density. Since the model assumes steady external conditions, these results show that unsteady nucleation can be the result of the coupling between interfacial supersaturation and nonlinear kinetics. Obviously, the characteristic times of nucleation rate oscillations resulting from the model and seen in the experiments differ significantly. We recall that during actual crystallization, transport is convective-diffusive, contrary to the assumption of purely diffusive transport in the simulations. This leads to shorter characteristic times of the transport towards the crystal's interface. Furthermore, frequent mechanic and hydrodynamic perturbations inevitably affect the transport processes during an experiment.

The step patterns emerging from the model are illustrated in Fig. 8, showing the evolution of the surface profile as snapshots separated by 30 min. After growth begins, two areas of low step density and a step bunch between them evolve. The step bunch is created by the second nucleation rate maximum at 250 min in Fig. 7. As the steps move to the right in this figure, the step bunches move with velocity close to that of the elementary steps. This regular behavior agrees with the expectations for the dynamics of noninteracting steps and corresponds to observations in Figs. 3(b) and 4. Further correspondence of the simulations results to the experimental observations can be found in the gradual steepening of the step trains segment, from mean $p \approx 0.0057$ to ≈ 0.0067, as well as in the tendency of decay of the step bunch. The phenomena of steepening and step-bunch decay as the steps move inwards are readily apparent in simulations of growth of crystals with larger top faces, $2a = 500\ \mu\text{m}$, where the steps pathway reaches $a = 250\ \mu\text{m}$.

To explain the discrepancy between the chaotic character of nucleation in Figs. 1 and 2 and the regular step patterns emerging in the model during nucleation, we recall that during real growth, a newly nucleated step lowers the surface supersaturation in a limited area on the crystal surface. Other nuclei can emerge near simultaneously in the vicinity of the newly nucleated step. As they spread and merge along the line between their centers, a pattern of parallel steps emerges. These steps interact via the competition for supply from the solution bulk along their length and self-organize into regular step patterns. In the two-dimensional model steps are nucleated as infinitely long and parallel, and the competition and its self-organizing role are turned on from the moment of nucleation. In this way, the model merges two stages in the evolution of the step trains: the step generation and self-organization upon parallelization.

Thus, the model results reproduce the main features of step-bunch evolution, observed in the experiments: step bunches appear due to unsteady surface nucleation of the new layers, as they move inwards they tend to decay and steepen and their velocity is close to the velocity of the elementary steps. Besides the chaotic step generation, the only features observed in the experiments, which the model fails to predict, are the twinning and the detwinning of the steps. Above, step twinning was assigned to the short-range step-step attraction, not included in the numerical model. The splitting of the twinned steps is discussed below.

F. Splitting of twinned steps due to lateral growth

The twinned steps in Figs. 3 and 4 are preserved over times of several minutes, during which they cover several micrometers. This observation is compatible with the existence of a short-range step-step attraction, which is stronger than potential elastic or entropic repulsion between the two elementary steps. If the net interaction is attractive it is unlikely that the detwinning is caused by thermal fluctuations or other random perturbations in the system. These considerations suggest that the detwinning cannot be explained via phenomena that equally affect a step along its length and are adequate for a linear model where each step is represented by a point interacting with its adjacent points. An example of detwinning involving variations in the shape of the step is provided below.

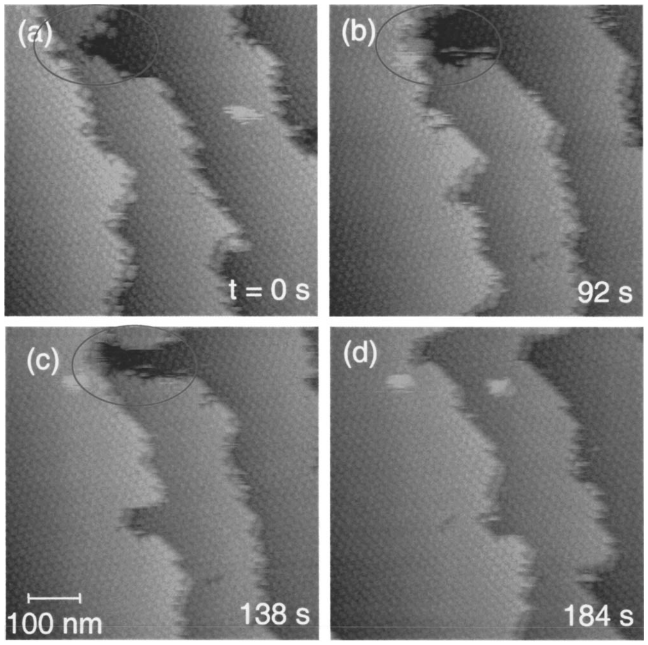

FIG. 9. Twinning and detwinning of steps at $\sigma = 1.6$ visualized by high-resolution atomic force microscopy. Time between frames is indicated in the images. Ellipse highlights step sections that twin and detwin due to lateral growth of the evolved channel.

Figure 9 presents an example of the evolution of two steps that twin and detwin during the observation period. Fig. 9(a) shows that twinning occurs when a section of the front step falls behind and finds itself at three molecular sizes from the rear step. A twinned segment, six or seven molecular sizes long is formed in Fig. 9(b), likely due to the attraction discussed above. This segment is joined to the front step by segments perpendicular to the main step direction in this step train. As growth proceeds, the side segments also grow in the lateral direction and narrow the channel between them in Fig. 9(c). When this channel eventually closes in Fig. 9(d), the front and the rear step have split.

The sequence of observations in Fig. 9 allows an estimate of the characteristic surface diffusion length of about three lattice parameters, in agreements with the estimate stemming from Fig. 3. Detwinning occurs because after the channel in direction perpendicular to that of the steps closes, the step separation is greater than the characteristic surface diffusion length.

ACKNOWLEDGMENTS

We thank N.A. Booth and O. Gliko for their critical reading of the manuscript and helpful suggestions. This work was supported by the Office of Biological and Physical Sciences, NASA, via Grant Nos. NAG8-1790, NAG8-1854, and NAG8-1824.

[1] I. Sunagawa and P. Bennema, J. Cryst. Growth **46**, 451 (1979); I. Sunagawa, in *Materials Science of the Earth's Interior,* edited by I. Sunagawa (Terra, Tokyo, 1984), p. 303; W. J. P. van Enckxevort, Prog. Cryst. Growth Charact. **9**, 1 (1984).

[2] A. A. Chernov, Y. G. Kuznetsov, I. L. Smol'sky, and V. N. Rozhanskii, Sov. Phys. Crystallogr. **31**, 705 (1986).

[3] E. D. Williams and N. C. Bartelt, Science **251**, 393 (1991).

[4] E. Bauser, in *Handbook of Crystal Growth*, edited by D. T. J. Hurle (North-Holland, Amsterdam, 1994), Vol. 3b, p. 879.

[5] P. G. Vekilov and J. I. D. Alexander, Chem. Rev. **100**, 2061 (2000).

[6] J. J. De Yoreo, N. P. Zaitseva, J. D. Lee, T. A. Land, I. Smolski, and E. B. Rudneva, J. Cryst. Growth **169**, 741 (1996); P. G. Vekilov and F. Rosenberger, Phys. Rev. E **57**, 6979 (1998); N. Zaitseva and L. Carman, Prog. Cryst. Growth Charact. Mater. **43**, 1 (2001).

[7] R. M. Tromp, F. M. Ross, and M. C. Reuter, Phys. Rev. Lett. **84**, 4641 (2000); J. Tersoff, *ibid.* **85**, 2843 (2000); P. Sutter and M. G. Lagally, *ibid.* **84**, 4637 (2000); M. Sato, M. Uwaha, and Y. Saito, Phys. Rev. B **62**, 8452 (2000).

[8] A. Pimpinelli, V. Tonchev, A. Videcoq, and M. Vladimirova, Phys. Rev. Lett. **88**, 206103 (2002).

[9] A. A. Chernov and T. Nishinaga, in *Materials Science of the Earth's Interior,* edited by I. Sunagawa (Terra, Tokyo, 1984), p. 207; S. R. Coriell, B. T. Murrary, A. A. Chernov, and G. B. McFadden, J. Cryst. Growth **169**, 773 (1996).

[10] A. A. Chernov, J. Cryst. Growth **118**, 333 (1992).

[11] M. Sato and M. Uwaha, Phys. Rev. B **51**, 11 172 (1995); M. Uwaha, Y. Saito, and M. Sato, J. Cryst. Growth **146**, 164 (1995).

[12] G. S. Bales and A. Zangwill, Phys. Rev. B **41**, 5500 (1990).

[13] J. P. Van der Eerden and H. Mueller-Krumbhaar, Electrochim. Acta **31**, 1007 (1986); J. P. Van der Eerden and H. Mueller-Krumbhaar, Phys. Rev. Lett. **57**, 2431 (1986).

[14] S. Y. Potapenko, J. Cryst. Growth **147**, 223 (1995).

[15] S. Stoyanov and V. Tonchev, Phys. Rev. B **58**, 1590 (1998).

[16] F. C. Frank, in *Growth and Perfection of Crystals,* edited by R. H. Doremus, B. W. Roberts, and D. Turnbul (Wiley, New York, 1958), p. 411.

[17] S. Stoyanov, Surf. Sci. **370**, 345 (1997).

[18] K. Chen and P. G. Vekilov, Phys. Rev. E **66**, 021606 (2002).

[19] D. N. Petsev, K. Chen, O. Gliko, and P. G. Vekilov, Proc. Natl. Acad. Sci. U.S.A. **100**, 792 (2003).

[20] D. N. Petsev, B. R. Thomas, S.-T. Yau, and P. G. Vekilov, Biophys. J. **78**, 2060 (2000); B. R. Thomas, D. Carter, and F. Rosenberger, J. Cryst. Growth **187**, 499 (1997).

[21] S.-T. Yau, D. N. Petsev, B. R. Thomas, and P. G. Vekilov, J. Mol. Biol. **303**, 667 (2000).

[22] S.-T. Yau, B. R. Thomas, and P. G. Vekilov, Phys. Rev. Lett. **85**, 353 (2000).

[23] D. N. Petsev, B. R. Thomas, S.-T. Yau, D. Tsekova, C. Nanev, W. W. Wilson, and P. G. Vekilov, J. Cryst. Growth **232**, 21 (2001).

[24] P. K. Hansma, J. P. Cleveland, M. Radmacher, D. A. Walters, P. Hillner, M. Bezanilla, M. Fritz, D. Vie, H. G. Hansma, C. B. Prater, J. Massie, L. Fukunaga, J. Gurley, and V. Elings, Appl. Phys. Lett. **64**, 1738 (1994); A. Noy, C. H. Sanders, D. V. Vezenov, S. S. Wong, and C. M. Lieber, Langmuir **14**, 1508 (1998).

[25] M. Giesen-Seibert, R. Jentjens, M. Poensgen, and H. Ibach, Phys. Rev. Lett. **71**, 3521 (1993); M. Poensgen, J. Wolf, J. Frohn, M. Giesen, and H. Ibach, Surf. Sci. **274**, 430 (1992); N. Kitamura, M. G. Lagally, and M. B. Webb, Phys. Rev. Lett. **71**, 2081 (1993).

[26] S.-T. Yau and P. G. Vekilov, Nature (London) **406**, 494 (2000).

[27] S.-T. Yau and P. G. Vekilov, J. Am. Chem. Soc. **123**, 1080 (2001).

[28] H. Lin, D. N. Petsev, S.-T. Yau, B. R. Thomas, and P. G. Vekilov, Cryst. Growth Design **1**, 73 (2001).

[29] A. Seeger, Philos. Mag. **44**, 348 (1953); W. R. Wilcox, J. Cryst. Growth **37**, 229 (1977).

[30] C. N. Nanev, Crystallogr. Rep. **3**, 1 (1993).

[31] A. A. Chernov, S. R. Coriell, and B. T. Murray, J. Cryst. Growth **132**, 405 (1993).

[32] A. A. Chernov, S. R. Coreill, and B. T. Murray, J. Cryst. Growth **149**, 120 (1995).

[33] P. G. Vekilov, J. I. D. Alexander, and F. Rosenberger, Phys. Rev. E **54**, 6650 (1996).

[34] P. G. Vekilov, B. R. Thomas, and F. Rosenberger, J. Phys. Chem. **102**, 5208 (1998).

[35] A. A. Chernov, J. Cryst. Growth **24/25**, 11 (1974).

[36] P. G. Vekilov, L. A. Monaco, and F. Rosenberger, J. Cryst. Growth **156**, 267 (1995); H. Lin, P. G. Vekilov, and F. Rosenberger, *ibid.* **158**, 552 (1996).

[37] P. G. Vekilov, H. Lin, and F. Rosenberger, Phys. Rev. E **55**, 3202 (1997).

[38] C. S. Haase, J. Chadam, D. Fenn, and P. Ortoleva, Science 209 (1980); C. J. Allegré, A. Provost, and C. Jaupart, Nature (London) **294**, 223 (1981); P. Gray and S. K. Scott, *Chemical Oscillation and Instabilities. Non-linear Chemical Kinetics* (Clarendon Press, Oxford, 1990); P. J. Ortoleva, *Geochemical Self-Organization* (University Press, Oxford, 1994).

[39] F. Rosenberger, H. Lin, and P. G. Vekilov, Phys. Rev. E **59**, 3155 (1999).

[40] P. G. Vekilov and F. Rosenberger, J. Cryst. Growth **158**, 540 (1996).

[41] D. M. Lawson, P. J. Artymiuk, S. J. Yewdall, J. M. A. Smith, J. C. Livingstone, A. Trefry, A. Luzzago, S. Levi, P. Arosio, G. Cesareni, C. D. Thomas, W. V. Shaw, and P. M. Harrison, Nature (London) **349**, 541 (1991); P. D. Hempstead, S. J. Yewdall, A. R. Fernie, D. M. Lawson, P. J. Artymiuk, D. W. Rice, G. C. Ford, and P. M. Harrison, J. Mol. Biol. **268**, 424 (1997).

[42] S. Toshev, A. Milchev, and S. Stoyanov, J. Cryst. Growth **13/14**, 123 (1972).

[43] P. G. Vekilov, F. Rosenberger, H. Lin, and B. R. Thomas, J. Cryst. Growth **196**, 261 (1999).